Title

Radiocesium interaction with clay minerals: Theory and simulation advances Post-Fukushima.

Authors

Okumura, Masahiko
Kerisit, Sebastien
Bourg, Ian C
et al.

Publication Date

2018-09-01

DOI

10.1016/j.jenvrad.2018.03.011

Peer reviewed

Radiocesium interaction with clay minerals: Theory and simulation advances Post–Fukushima

Masahiko Okumura[a,*], Sebastien Kerisit[b], Ian C. Bourg[c], Laura N. Lammers[d,e], Takashi Ikeda[f], Michel Sassi[b], Kevin M. Rosso[b], Masahiko Machida[a]

[a] Center for Computational Science and e-Systems, Japan Atomic Energy Agency, Kashiwa, Chiba 277-0871, Japan [b] Physical Sciences Division, Pacific Northwest National Laboratory, Richland, WA 99354, USA [c] Department of Civil and Environmental Engineering and Princeton Environmental Institute, Princeton University, Princeton, NJ 08544, United States [d] Department of Environmental Science, Policy, and Management, University of California, Berkeley, CA 94720, United States [e] Earth and Environmental Science Area, Lawrence Berkeley National Laboratory, Berkeley, CA 94720, United States [f] Synchrotron Radiation Research Center, Quantum Beam Science Research Directorate (QuBS), National Institutes for Quantum and Radiological Science and Technology (QST), Sayo, Hyogo 679-5148, Japan

∗ Corresponding author. E-mail address: okumura.masahiko@jaea.go.jp (M. Okumura).

ABSTRACT

Insights at the microscopic level of the process of radiocesium adsorption and interaction with clay mineral particles have improved substantially over the past several years, triggered by pressing social issues such as management of huge amounts of waste soil accumulated after the Fukushima Dai–ichi nuclear power plant accident. In particular, computer–based molecular modeling supported by advanced hardware and algorithms has proven to be a powerful approach. Its application can now generally encompass the full complexity of clay particle adsorption sites from basal surfaces to interlayers with inserted water molecules, to edges including fresh and weathered frayed ones. On the other hand, its methodological schemes are now varied from traditional force–field molecular dynamics on large–scale realizations composed of many thousands of atoms including water molecules to first–principles methods on smaller models in rather exacting fashion. In this article, we overview new understanding enabled by simulations across methodological variations, focusing on recent insights that connect with experimental observations, namely: 1) the energy scale for cesium adsorption on the basal surface, 2) progress in understanding the structure of clay edges, which is difficult to probe experimentally, 3) cesium adsorption properties at hydrated interlayer sites, 4) the importance of the size relationship between the ionic radius of cesium and the interlayer distance at frayed edge sites, 5) the migration of cesium into deep interlayer sites, and 6) the effects of nuclear decay of radiocesium. Key experimental observations that motivate these simulation advances are also summarized. Furthermore, some directions toward future solutions of waste soil management are discussed based on the obtained microscopic insights.

1. Introduction

The 2011 Great East Japan Earthquake (Japan Meteorological Agency, 2011) and subsequent tsunami caused a severe accident at the Fukushima Dai–ichi Nuclear Power Plant (FDNPP) (International Atomic Energy Agency, 2015), which released huge amounts of radioactive nuclides into the environment (Yoshida and Takahashi, 2012; Mikami et al., 2015; Ministry of Education, Culture, Sports, Science and Technology, 2011). Among the released radionuclides, the foremost contributor to radioactive exposure in the region surrounding the power plant is ^{137}Cs, which has a half–life of 30.1 years and a strong tendency to bind to soil fine particles. Over the last seven years, the Japanese Government has led an extensive decontamination campaign aimed particularly at decreasing exposure to ^{137}Cs (Ministry of Environment, 2011). The standard procedure –the removal of top soil– has proven arduous yet effective at reducing air dose rates and the area of the evacuation zone (Japan Atomic Energy Agency, 2014a, 2014b; Miyahara et al., 2015).

A new issue, however, has arisen as a by–product of this success: namely, a tremendous amount of waste soil (about 15,600,000 m^3) has accumulated in temporary storage facilities (Ministry of Environment, 2011). In response to this issue, the Japanese Government created an interim storage facility surrounding the FDNPP while announcing plans to commission a permanent disposal site outside the Fukushima Prefecture (Ministry of Environment, 2011). Implementation of the final disposal plan, however, requires that the waste volume be significantly reduced to minimize the costs and safety challenges associated with site construction, waste transportation, and long–term site management. These challenges have motivated renewed efforts to develop volume reduction schemes for Cs–contaminated soils. To date, however, no scheme has yet been demonstrated to perform suitably at scale in real field conditions. A major reason is the absence of scientific consensus regarding the binding mechanisms, thermodynamics, and kinetics of Cs in complex soils and sediments.

This lack of consensus derives partly from the inherent complexity of soils and partly from the fact that Cs adsorption in natural environments involves multiple binding sites, the most important of which have very low density, very high affinity, and complex kinetics of cesium uptake and release. The very low density of these sites makes them challenging to observe and characterize even using the most cutting–edge microscopic techniques. To overcome these constraints, computational microscopic simulations have proven useful (Kubicki, 2016) with particularly rapid advancement of computing resources since the earliest investigations (e.g., Smith, 1998; Young and Smith, 2000; Rosso et al., 2001). For example, classical molecular dynamics (MD) techniques can reveal the collective behaviors of thousands of atoms at the clay–water interface and can now account for the effects of particle morphology (Lammers et al., 2017). Moreover, first–principles MD (FPMD) techniques, though restricted to smaller system sizes, have been

widely employed due to their strong transferability to various situations without the need for deriving force field models.

Here we review recent developments in microscopic understanding of Cs adsorption on clay minerals given by state–of–the–art computational molecular simulations. In particular, the last five years after the FDNPP accident have seen significant advances. In the remainder of this article, we introduce key techniques, summarize the insights gained, and discuss their implications for waste volume reduction.

2. An overview of Cs adsorption on illite

The adsorption and fixation of radiocesium to fine particles has been a recurrent question since the dawn of the nuclear age (Sawhney, 1972; Cornell, 1993; Delvaux et al., 2000). One of the most important findings is that illite, a micaceous clay mineral that is common in soils and sediments, is a particularly strong adsorbent of Cs. In this section, we give a brief review of Cs adsorption on illite as characterized using experimental studies at various scales.

2.1. Macroscopic scale

Batch experiments have revealed that Cs adsorption on illite shows a Freundlich–type isotherm (Brouwer et al., 1983; Staunton and Roubaud, 1997; Poinssot et al., 1999; Bradbury and Baeyens, 2000; Zachara et al., 2002; Liu et al., 2003; Steefel et al., 2003; Goto et al., 2008), which implies the existence of multi–component adsorption sites. Actually, the isotherm can be interpreted as a superposition of several isotherms (Brouwer et al., 1983; Poinssot et al., 1999; Bradbury and Baeyens, 2000; Zachara et al., 2002; Liu et al., 2003; Steefel et al., 2003). The adsorption sites corresponding to these isotherms are often referred as type–I, -II, …, sites, whereby lower numbers correspond to sites with stronger affinity and lower capacity, i.e., sites that dominate adsorption at progressively lower Cs loadings. For example, the type–I site has the lowest capacity (only ~ 0.25% of the total cation exchange capacity (CEC) of illite) but contributes predominantly to Cs adsorption at concentrations below 10^{-8} M Cs (Bradbury and Baeyens, 2000). These sites are referred to hereafter as “macroscopic model sites”. It has been shown that Cs adsorb selectively at these sites against competitive cations (Na^+, K^+, Rb^+, NH_4^+, Ca^{2+}, etc.), i.e., all sites adsorb Cs selectively with the order of strength as type–I > -II > … (Sawhney, 1972; Comans et al., 1991; Brouwer et al., 1983; Poinssot et al., 1999; Bradbury and Baeyens, 2000; Zachara et al., 2002). Based on this Cs selectivity, a useful quantity, referred to as radiocaesium interception potential (RIP), was introduced to estimate the amount of highly selective sites (Cremers and Pleysier, 1973; Wauters et al., 1996). The kinetics of Cs adsorption and desorption have also been studied at the macroscopic scale (Comans et al., 1991; Comans and Hockley, 1992; Poinssot et al., 1999; Zachara et al., 2002; Liu et al., 2003; de Koning and Comans, 2004). A notable outcome of these studies is that a longer initial contact time with the

Cs–bearing solution (aging time) decreases the amount of extractable Cs from all sites (Evans et al., 1983; Wauters et al., 1994; de Koning and Comans, 2004).

2.2. Mesoscopic scale (~nm)

A well known limitation of geochemical speciation models is that regardless of their agreement with macroscopic adsorption data they cannot, on their own, unambiguously constrain the physical and chemical details of individual adsorption sites. Nevertheless, macroscopic scale data have guided the development of mesoscopic conceptual models that attempt to explain key features of the macroscopic scale data (Jackson, 1963). The conceptual model of an illite particle shown in Fig. 1 illustrates the five types of adsorption sites that are thought to exist on this mineral. These sites, referred to hereafter as “structural adsorption sites”, are the basal surface (planar) site, edge site, hydrated interlayer site, frayed edge site (FES), and anhydrous interlayer site. The conceptual model shown in Fig. 1 is consistent with images of individual illite particles observed using transmission electron microscopy (TEM) (Fuller et al., 2015).

Comparison between the area of the structural adsorption sites and the adsorption capacity of the different macroscopic model sites suggests that the frayed edge and basal sites hypothesized to occur at the mesoscopic scale correspond to the type–I and -III sites used in three–site macroscopic scale adsorption models (i.e., the sites with the smallest and largest Cs adsorption capacity) (Brouwer et al., 1983). This inference is further supported by observations indicating that Cs adsorbs primarily near illite edge surfaces at low loadings (Rajec et al., 1999; McKinley et al., 2004) and on the basal surface at high loadings (Kim et al., 1996).

A particularly interesting feature of the conceptual model described in Fig. 1 is that it has the potential to explain the complex kinetics of Cs adsorption on illite. For example, reports of irreversible Cs adsorption may reflect the collapse of hydrated interlayers or the migration of Cs into core region of illite particles (Jacobs and Tamura, 1960; Sawhney, 1972; de Koning and Comans, 2004), two mechanisms that are supported by TEM observations (Okumura et al., 2014b; Fuller et al., 2015).

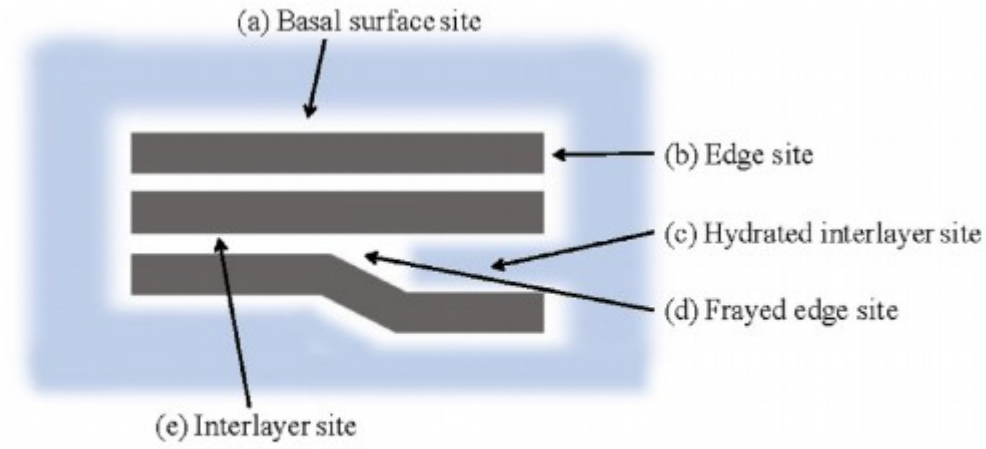

Fig. 1. Conceptual model of adsorption sites on an illite particle. This model contains (a) basal surface, (b) edge, (c) hydrated interlayer, (d) frayed edge, and (e) interlayer sites.

2.3. Microscopic scale (~Å)

Although the mesoscopic model outlined above is consistent with various features of Cs adsorption on illite, additional microscopic physical/chemical insight is needed to develop a truly predictive understanding as required, e.g., to develop efficient Cs extraction methodologies. Until about 15 years ago, such nanoscale insight was limited to a few experimental results revealing the atomistic level coordination of adsorbed Cs in a small range of conditions. In particular, NMR experiments showed the existence of two distinct Cs adsorption sites on illite particles (Kim and Kirkpatrick, 1997), while extended X–ray adsorption fine structure spectroscopy (EXAFS) data yielded estimates of the average distribution of Cs–O distances in the first coordination shell of adsorbed Cs (Bostick et al., 2002).

3. Progress in experiments since the Fukushima accident

In this section, we give a brief review of relatively recent experimental insights into Cs binding in clay particles motivated by the FDNPP accident. In particular, we highlight experiments that provide a more robust basis for the molecular modeling studies discussed in the rest of this paper.

One of the most important observations regarding radiocesium adsorption in Fukushima soils is that weathered biotite is a primary adsorbent (Yamada et al., 2014; Mukai et al., 2014, 2016a, 2016b; Kikuchi et al., 2015). For example, recent experiments showed that illite and weathered biotite are the primary radiocesium–bearing phases in silt- and sand–size fractions of Fukushima soil (Tanaka et al., 2018). Note that biotite in this article is defined as a Fe–rich phlogopite and/or a Mg–rich annite with the chemical formula $K(Mg,Fe)_3AlSi_3O_{10}(F,OH)$ as identified by X–ray diffraction (XRD), energy dispersive X–ray spectrometry (EDS) and TEM (Kikuchi et al., 2015; Mukai et al., 2016a). Although some observations prior to the Fukushima

accident had identified the potential importance of weathered biotite as a Cs adsorbent (Sawhney, 1966; McKinley et al., 2001, 2004; Zachara et al., 2002), this observation is particularly critical in the Fukushima case because weathered granite, which contains weathered biotite, is a dominant source rock in the Fukushima area (Kikuchi et al., 2015; Mukai et al., 2016b; Takahashi et al., 2017). Despite the structural similarity between biotite and illite, macroscopic experiments showed that biotite has stronger affinity of Cs than illite (Mukai et al., 2016b).

Important insight into Cs adsorption in Fukushima soils is provided by XRD and TEM observations of Cs uptake on weathered biotite and vermiculite (a related phyllosilicate with high structural charge density). In particular, Cs readily incorporates in anhydrous vermiculite interlayers and tends to segregate itself by almost full monoionic replacement in some interlayer spaces (Kogure et al., 2012). Furthermore, exposure to artificially high Cs concentrations was shown to cause a collapse (dehydration) of the interlayers of weathered biotite collected from the Fukushima Prefecture (Kikuchi et al., 2015). Finally, small–angle X–ray scattering (SAXS) studies revealed differences between the mesoscopic structural changes of vermiculite and weathered biotite caused by Cs adsorption (Motokawa et al., 2014a); in particular, experimental results indicate that weathered biotite contains wedge–- shape interlayer structures, i.e., FES structures similar to those of illite (Fig. 1). Motokawa et al. (2014b) also showed details of collective structural changes of vermiculite caused by Cs adsorption.

Local atomic environments around adsorbed Cs in clay minerals have been measured primarily using X–ray absorption spectroscopy methods. EXAFS studies of additional Cs adsorbed to natural samples of actual Fukushima soil revealed that the local structure surrounding Cs is very close to ones in mica and that Cs in Fukushima soils forms both of inner- and outer–sphere surface complexes (Qin et al., 2012). The observed interlayer collapse due to migration of Cs in vermiculite extracted from actual Fukushima soils (Tsuji et al., 2014) is thought to originate from the low hydration energy of Cs, which is reflected as a poor organization of water molecules around the hydrated Cs ion (Ikeda and Boero, 2012; Machida et al., 2015). EXAFS studies of the impact of pH on the atomic environment around Cs in vermiculite indicate that inner–sphere complexes become increasingly more predominant as pH increases from 3.0 to 7.0 (Fan et al., 2014a). Fan et al. (2014b) found a correlation between the availability of strong adsorption sites and the ratio of inner–sphere complexes with respect to both (inner- and outer–sphere) complexes in illite, vermiculite, and montmorillonite by a study on relation between EXAFS analysis and RIP evaluation. Real–time–resolved EXAFS revealed rapid adsorption of Cs on vermiculite (Matsumura et al., 2014). Using near–edge XAFS, the influence of water molecule coordination on the chemical state of unoccupied molecular orbitals in Cs was examined (Honda et al., 2016).

4. Progress in microscopic modeling

Atomistic simulations using Monte Carlo (MC), classical MD, and density functional theory (DFT) techniques have played an important role in elucidating the structure and reactivity of clay minerals on a microscopic scale (Kubicki, 2016), in concert with experimental and theoretical studies (Liebau, 1985; Mottana et al., 2002). The importance and utility of these methods is illustrated, for example, by the existence of multiple sets of interatomic potential parameters developed for classical MD simulations of clay minerals (Skipper et al., 1989; Cygan et al., 2004; Heinz et al., 2005; Sakuma and Kawamura, 2011; Pitman and van Duin, 2012; Tesson et al., 2016). To date, however, much of the atomistic simulation effort has focused on the basal surfaces of smectite and kaolinite clay minerals rather than on the edges, frayed edges, and interlayers of illite and weathered biotite.

From a molecular modeling perspective, illite and weathered biotite are likely to have common site–specific properties. Both minerals are thought to have a common mesoscopic structure characterized by the five sites shown in Fig. 1. In addition, both minerals have similar chemical formulae: $K_{1-x}Al_2(Si_{3-x}Al_x)O_{10}(F,OH)_2$ ($0 < x < 1$) and $K_{1-x'}(Mg_{3-\alpha}Fe_{\alpha-x'}^{2+}Fe_{x'}^{3+})(Si_3Al)O_{10}(F,OH)_2$ ($0 < \alpha < 3$ and $0 \leq x' \leq \alpha$) in the case of illite and biotite, respectively. The major crystallographic difference is that the octahedral sheets of illite and biotite are di- and tri–octahedral, respectively. Though this difference in octahedral sheet occupancy may cause some difference in the adsorption properties of the two minerals, illite is often used as a representative model for both minerals. In some cases, phlogopite has been used a convenient tri–octahedral proxy for weathered biotite. Advances in the atomistic level modeling of the adsorption sites of illite, phlogopite and related minerals is reviewed below.

4.1. Basal surface site

As discussed in section 2, NMR experiments have revealed that Cs can adsorb on the basal surface in significant proportions (Kim et al., 1996). Subsequently, advances in experimental and theoretical techniques have led to the determination of the energetics of Cs adsorption as well as the atomic–scale structure of adsorbed Cs ions and interfacial water molecules at the basal surface.

The basal surface has a simple flat structure that facilitates measurements with techniques such as X–ray reflectivity (XRR) and atomic force microscopy (AFM). Consequently, ion adsorption phenomena on the basal surfaces of phyllosilicates have been extensively studied (Lee et al., 2012, 2013, 2017; Pintea et al., 2016; Araki et al., 2017). In particular, detailed experimental data have been reported on the distribution of Cs ions above the basal surface (Lee et al., 2012, 2013; Pintea et al., 2016; Araki et al., 2017).

Molecular simulations are well–suited to study in isolation the individual factors that control Cs adsorption (Vasconcelos et al., 2007; Sakuma and Kawamura, 2011; Bourg and Sposito, 2011; Kerisit et al., 2016; Loganathan and Kalinichev, 2017; Bourg et al., 2017). For example, Kerisit et al. (2016)

used classical MD simulations to systematically study the effect of the magnitude and location of the permanent charge on the free energy of Cs adsorption on phyllosilicate basal surfaces (Fig. 2) for a range of model phyllosilicates (pyrophyllite, illite, muscovite, phlogopite, celadonite, and margarite). In addition to a shallow minimum associated with outer–sphere adsorption, all phyllosilicates, except pyrophyllite, showed a strong preference for adsorption as an inner–sphere complex, whereby Cs^+ adsorbed directly above a six–membered ring cavity and was coordinated to six surface oxygen atoms and five to six water molecules (Kerisit et al., 2016). The simulations further revealed a linear correlation between the magnitude of the layer charge and the free energy of formation of the inner–sphere complex (Kerisit et al., 2016). The structure of the octahedral layer and the distance to neighboring surface K^+ ions were also found to have a significant influence on the adsorption free energy; for example, Cs adsorption was found to be more favorable on muscovite than on phlogopite, because the tri–octahedral sheet structure of the latter leads to a shorter hydroxide H–Cs distance than the di–octahedral sheet of the former (Kerisit et al., 2016). More recently, Loganathan and Kalinichev (2017) showed that the location of aluminum substitutions within the surface tetrahedral layer affects the adsorption free energy of Cs. Finally, MD simulations by Bourg et al. (2017) were found to accurately reproduce experimental X–ray reflectivity data on the structure of water on a Cs–bearing basal surface of muscovite mica as well as experimental data on the free energy of exchange between Na, K, Rb, and Cs. Overall, these recent numerical simulations reveal that the atomic–scale structure of the basal surface significantly modulates Cs adsorption affinity.

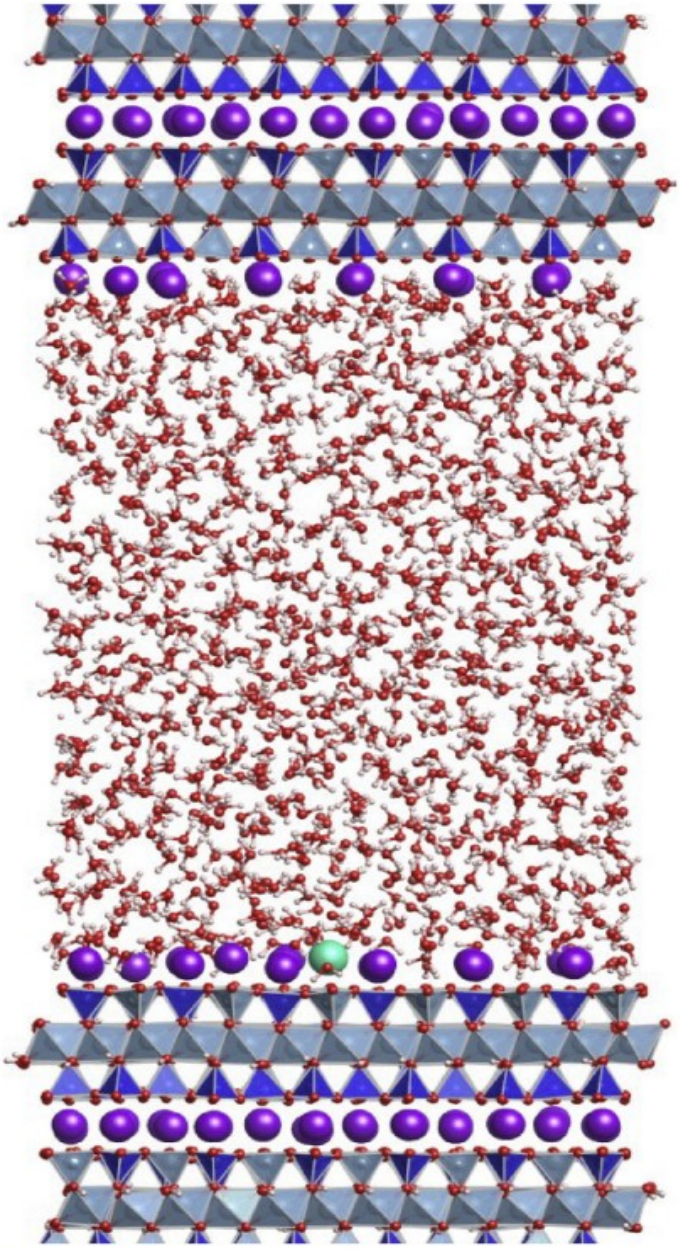

Fig. 2. Snapshot from a typical molecular dynamics simulation of a phyllosilicate–water interface with Cs^+ adsorbed as an inner–sphere complex (green sphere). SiO_4 tetrahedra are shown in dark blue, AlO_4 and AlO_6 polyhedra in light blue, and O, H, K, and Cs atoms are shown by red, light pink, purple, and light green spheres, respectively. (For interpretation of the references to color in this figure legend, the reader is referred to the Web version of this article.)

4.2. Edge sites

The edge surfaces of clay minerals on a microscopic scale have been extensively studied because of their important roles in protonation/deprotonation, dissolution/growth, and adsorption of transition metals and oxyanions. In the specific case of Cs adsorption by (and extraction from) micaceous minerals, they are of interest particularly because of their role in the formation of hydrated interlayer sites with/without FES (Fuller et al.,

2015), in the dissolution of the clay framework (Kuwahara, 2006), and potentially as a distinct adsorption site (Lammers et al., 2017). Despite the importance of clay edge surfaces, however, their exact structure remains incompletely understood (Meunier, 2006), in part because the preferred crystallographic orientation of clay edges is sometimes challenging to observe (Bourg et al., 2007; Tournassat et al., 2016).

In the absence of experimentally established edge crystallographic structures, computational and theoretical studies have played an important role in generating plausible models. Almost all of these studies have relied on the initial assumption that the ratio of octahedrally-to tetrahedrally–coordinated cations at the edge surface is identical to that in the bulk crystal despite experimental evidence that the edge surfaces of clay minerals exposed to low- or high–pH solutions may become enriched in Si or Al, respectively (Carroll and Walther, 1990). Within the framework of this assumption, the picture that emerges from DFT calculations of dry and hydrated clay edge surfaces is consistent with the predictions of earlier periodic bond chain theory calculations (White and Zelazny, 1988): the most stable edge surfaces correspond to the (110) and (010) crystallographic planes (Churakov, 2006; Kwon and Newton, 2016); the edge surfaces carry significantly under- or over–coordinated edge O atoms that are stabilized by bond–length relaxation such that the edges are essentially uncharged at near–neutral conditions (Bickmore et al., 2003; Liu et al., 2014; Tournassat et al., 2016); finally, octahedral Al atoms exposed at clay edge surfaces can readily become five–coordinated through the detachment of an -OH2 functional group (Liu et al., 2015; Lammers et al., 2017; Okumura et al., 2017).

Few molecular simulation studies have investigated the sorption of Cs^+ to edges of layered silicate minerals. MD simulations of Cs sorption to the neutral (110)–edge of K–illite show that Cs ions form predominantly inner–sphere complexes located in the same plane and relative position as interlayer K ions, such that the edge sorption site resembles a continuation of the interlayer (Lammers et al., 2017). Excess Cs sorption is greatest adjacent to edge sites with comparatively lower charge density. Ion exchange selectivity between Cs and Na at edge sites increases with decreasing Cs content, with a maximum value of log $K^{Na/Cs}$ of ~1.4. Thus, edge sites have intermediate Na/Cs ion exchange selectivity coefficients compared to the basal surface sites and frayed edge or interlayer sites, which are discussed in section 4.4 and 4.5.

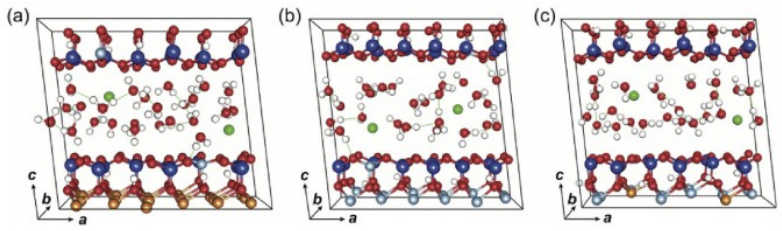

Fig. 3. Snapshots of (a) Cs–Sap, (b) Cs–Bei, and (c) Cs–Mnt taken from preparation runs under constant *NPT* conditions of $P = 1$ atm and $T = 300$ K (Ikeda et al., 2015). Atom colors of O, H, K, and Cs atoms are red, light pink, purple, and light green spheres, respectively. (For interpretation of the references to color in this figure legend, the reader is referred to the Web version of this article.)

4.3. Hydrated interlayer sites

Pioneering works using MC and MD simulations showed several fundamental properties of Cs ions in hydrated smectite interlayers, e.g., swelling properties, formation of inner–sphere complex of Cs ions, diffusion coefficients of Cs, etc. (Smith, 1998; Shroll and Smith, 1999; Young and Smith, 2000; Sutton and Sposito, 2001, 2002; Marry et al., 2002, 2008; Marry and Turq, 2003; Whitley and Smith, 2004; Rotenberg et al., 2007; Kosakowski et al., 2008; Liu et al., 2008; Zheng and Zaoui, 2011; Zheng et al., 2011; Ngouana and Kalinichev, 2014).

To gain a deeper insight into the adsorption states of hydrated interlayer cations in clay minerals, model systems have been used for FPMD simulations. Ikeda et al. (2015) performed a series of constant pressure FPMD simulations at P = 1 atm and T = 300 K for the three kinds of 2:1 type clay minerals corresponding to saponite (Sap), beidellite (Bei), and montmorillonite (Mnt) containing alkali cations in the interlayer. Fig. 3 shows the resultant structural modes of Cs–Sap, Cs–Bei, and Cs–Mnt clays, each of which has formally the same amount of layer charge of -e/3 per $O_{10}(OH)_2$ introduced by the isomorphic substitution, typical of the smectite group.

Then, Ikeda et al. (2015) investigated systematically the adsorption states of alkali cations in their swelling clay minerals via FP–metadynamics (MTD) simulations (Laio and Parrinello, 2002; Iannuzzi et al., 2003). Fig. 4 shows the reconstructed free energy profile ΔF representing the adsorption states of Na^+ and Cs^+ in the interlayer of Sap clays obtained from their FP–MTD simulations along with the adsorption structure corresponding to its minimum. The computed ΔF shows that an inner–sphere complex is preferentially formed for Cs^+ in the interlayer of Sap, whereas an outer–sphere complex tends to be formed for Na^+ instead. Such strong preference for an inner–sphere complex of Cs^+ observed in Sap is not shown in Bei and Mnt, indicating that the reactivity of O_b atoms in tetrahedral sheets varies significantly depending on the detailed composition of 2:1 type clay minerals even if they have the same amount of layer charge. Indeed, the local density of states (LDOS) lying just below Fermi level (E_F) at O_b sites differ significantly among the three model clays as shown in Fig. 5, where the corresponding LDOSs at the neighboring apical O (O_a) sites are also shown for comparison. The observed variation of LDOS just below E_F suggests that the Lewis basicity of O_b atoms decreases in the order of Sap > Bei > Mnt in good accordance with that of the affinity of Cs^+ with O_b atoms suggested from FP–MTD simulations. Furthermore, the Cs–O_b interactions in the inner–sphere complex preferentially formed in Sap–like clays include non–negligible covalency resulting mainly from the electron donation from O_b 2p to Cs^+ 5d empty orbitals. In addition, Cs^+ aggregation is suggested to occur in hydrated regions between Fe^{3+}–rich clay layers in weathered biotites from FPMD simulations (Ikeda, 2016) performed by employing model systems containing Fe^{3+} ions rather than Fe^{2+} and a certain quantity of vacancies in

octahedral sheets, which are known to result from the chemical weathering of biotite.

4.4. Frayed edge sites

As noted above, FES are often invoked as the possible origin of the very strong affinity of Cs for illite and weathered biotite at very low loadings. These sites are characterized by the existence of a “wedge–- shaped” nanopore structure in regions where the phyllosilicate layers transition from anhydrous to hydrated interlayers (Jackson, 1963). Strong Cs adsorption at these sites is generally though to result from the low hydration free energy of Cs, though some studies have pointed out that the low hydration energy of Cs does not fully explain its highly selective adsorption (Brouwer et al., 1983).

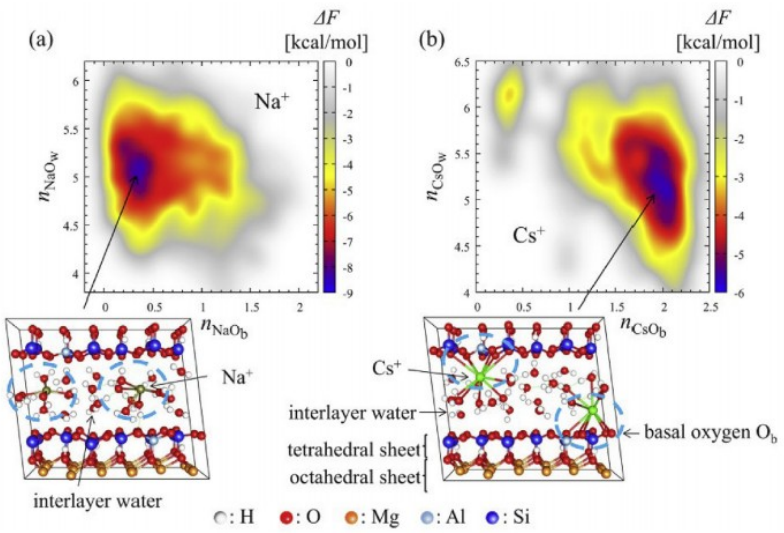

Fig. 4. ΔF representing the adsorption states of (a) Na^+ and (b) Cs^+ in the interlayer of Sap clays obtained from FP–MTD and the adsorption structure corresponding to its minimum (Ikeda et al., 2015). Atom colors of O, H, K, Na, and Cs atoms are red, light pink, purple, gray, and light green spheres, respectively. (For interpretation of the references to color in this figure legend, the reader is referred to the Web version of this article.)

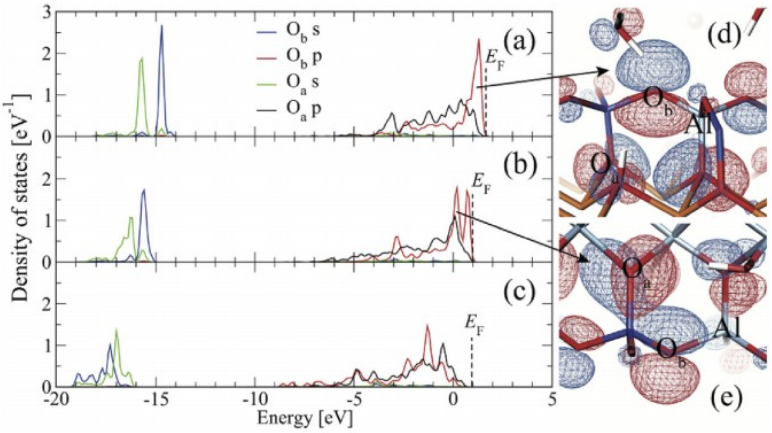

Fig. 5. LDOSs at selected O_a and O_b atoms in (a) Cs–Sap, (b) Cs–Bei, and (c) Cs–Mnt clays (Ikeda et al., 2015). The orbital corresponding to a peak located at 1.1 eV in (a) and at 0.1 eV in (b) is represented as wire–frames in (d) and (e), respectively.

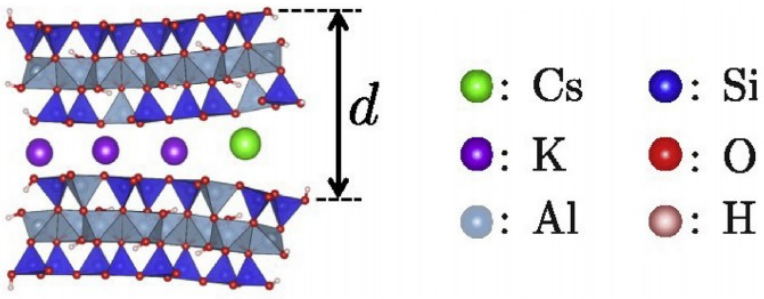

Fig. 6. Toy model of FES (Okumura et al., 2013). SiO_4 tetrahedra are shown in dark blue, AlO_4 and AlO_6 polyhedra in light blue, and O, H, K, and Cs atoms are shown by red, light pink, purple, and light green spheres, respectively. The ion exchange energies are evaluated varying the interlayer distance *d*. (For interpretation of the references to color in this figure legend, the reader is referred to the Web version of this article.)

In order to gain insight into the K–Cs exchange selectivity of FES, Okumura et al. (2013) constructed a toy model as shown in Fig. 6, in which free energy of K–Cs exchange between FES and liquid water was predicted as a function of a distance *d* characterizing the degree of opening of the FES. The definition can be represented as follows,

$$\Delta F = (E_{\mathrm{FES}}(\mathrm{Cs}^+;\ d) + G_{\mathrm{hyd}}(\mathrm{K}^+)) - (E_{\mathrm{FES}}(\mathrm{K}^+;\ d) + G_{\mathrm{hyd}}(\mathrm{Cs}^+)) \qquad (1)$$

where $E_{\mathrm{FES}}(A^+; d)$ is the energy of the FES model system with A^+ ion and interlayer distance *d*, which is evaluated by DFT calculation without any thermal effects for simplicity, and $G_{\mathrm{hyd}}(B^+)$ is the experimental hydration energy of ion B^+ (Okumura et al., 2013). The result (Fig. 7) showed that Cs is preferentially adsorbed by FES, relative to K^+, only when d becomes larger than 1.1 nm. The energy difference reaches −23 kJ/mol at d = 1.3 nm, which is consistent with the experimentally–derived value of −27 kJ/mol (Brouwer et al., 1983). This quantitative agreement suggests that this model succeeded in capturing an aspect of FES.

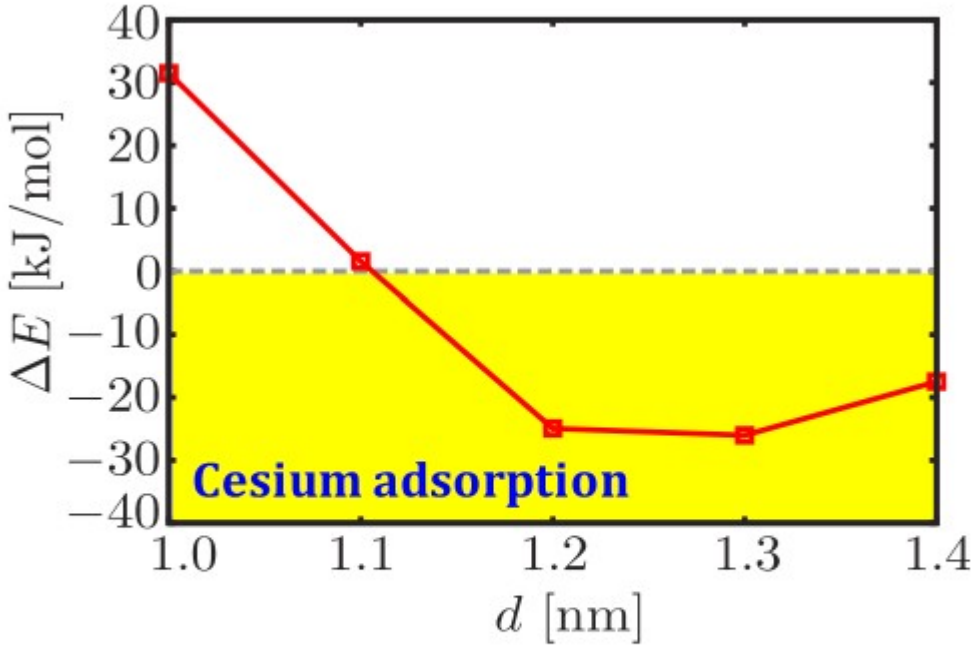

Fig. 7. The ion exchange energy against K in FES vs the interlayer distance of FES (Okumura et al., 2013). Horizontal and vertical axes represent the interlayer distance d nm and the ion exchange energy ΔE kJ/mol. The yellowed region is a guide for negative ion exchange energy.

The origin of the result shown in Fig. 7 can be interpreted as a combination of size matching between the ionic radius of the adsorbing ion and the interlayer distance and the difference in hydration energies of Cs and K (Okumura et al., 2013). This interpretation is explained by the following decomposition of Eq. (1),

$$\Delta E = (E_{\mathrm{FES}}(\mathrm{Cs}^+;\ d) - E_{\mathrm{FES}}(\mathrm{K}^+;\ d)) - (G_{\mathrm{hyd}}(\mathrm{Cs}^+) - G_{\mathrm{hyd}}(\mathrm{K}^+)) = \Delta E_{\mathrm{site}} - \Delta E_{\mathrm{hyd}} \quad (2)$$

where ΔE_{site} and ΔE_{hyd} represent the energy difference between FES with Cs and potassium and the hydration energy difference, respectively. This equation clearly illustrates that the difference in hydration energies (ΔE_{hyd}) does not fully explain the strong adsorption of Cs to FES; the difference in the free energy of interaction between each cation and the adsorption site (ΔE_{site}) is also critical.

More recently, MD simulations of FES were performed with a large model of Al–hydroxy interlayered vermiculite, which also has the wedge structure (Zaunbrecher et al., 2015). This model has hydrated interlayer sites, in contrast, the DFT model represents only the wedge structure without hydrated interlayer sites. This analysis gives consistent results with the DFT

calculations, i.e., adsorption of larger cations such as Cs and Rb can be energetically highly favored at FES.

4.5. Interlayer sites

Anhydrous interlayer sites of the 2:1 layered silicates are the final and most elusive adsorption sites in radiocesium–contaminated soils. The study of ion exchange involving interlayer sites has a long history (Barshad, 1954; Scott and Smith, 1966; Reichenbach and Rich, 1969; Sawhney, 1972; Sánchez–Pastor et al., 2010). Many studies have shown that exchange of K+ for ions with relatively large hydration enthalpies, including Na^{+}, Ba^{2+}, Sr^{2+}, Ca^{2+} and the hydronium ion (Rausell–Colom et al., 1965; Quirk and Chute, 1968; Reichenbach and Rich, 1968, 1969; Sánchez–Pastor et al., 2010), lead to layer expansion or “decollapse”. However, the presence of even trace amounts of aqueous K^{+} or NH_4^{+} in solution can strongly inhibit exchange by solvated counterions (Scott et al., 1960; Scott and Smith, 1966) due to the strong thermodynamic penalty for replacement of K^{+} by hydrated ions in the interlayer (Rausell–Colom et al., 1965). On the other hand, Cs^{+} migration into deep anhydrous interlayer sites without “decollapse” has been observed (Okumura et al., 2014b; Fuller et al., 2015). In addition, the exchangeability of Cs adsorbed to natural weathered vermiculite is highly limited even in strong acid, and it decreases over time (Mukai et al., 2016b).

Based on these observations, there are two candidate pathways by which Cs can enter and become “fixed” in the interlayer region (1) decollapse–driven exchange, and (2) direct exchange (Fig. 8). Simulations of Na–montmorillonite showed low energy barriers for Cs and Na migration from the micropore into hydrated interlayer nanopores (Rotenberg et al., 2009) and relatively rapid diffusion of Cs in hydrated interlayers (Marry and Turq, 2003; Kosakowski et al., 2008; Bourg and Sposito, 2010). These results illustrate that Cs can exchange rapidly with interlayer Na in 2–layer Na–montmorillonite, and likely cannot explain the decreasing exchangeability of interlayer Cs with time (Evans et al., 1983; Wauters et al., 1994; de Koning and Comans, 2004).

Direct exchange is the replacement of anhydrous interlayer (non–-exchangeable) K by Cs without a decollapsed (hydrated) intermediate. To investigate the feasibility and pathway of the direct exchange mechanism, Ruiz Pestana et al. (2017) performed MD simulations and DFT calculations that quantified the impact of Cs ions on the mobility of interlayer K in illite. They found that ion diffusion in anhydrous interlayers is likely controlled by ion migration between neighboring counterion sites, and that the magnitude of the energy barrier is controlled by the local basal spacing or Cs content. The K ions located in the vicinity of larger Cs^{+} in the anhydrous interlayer have significantly lower ion migration barriers than K ions in pure K–illite, accelerating K diffusion by orders of magnitude. These simulations suggest that energy barrier lowering by the larger Cs ions promotes subsequent K ion exchange events, allowing the direct exchange of K by Cs to proceed in the

absence of interlayer water (Ruiz Pestana et al., 2017). On the other hand, the decollapse mechanism appears to play a crucial role in the case of radiocesium adsorption in divalent cation rich solutions (Benedicto et al., 2014). Therefore, the critical mechanism of radiocesium migration in the anhydrous interlayer (“direct exchange” or “decollapse”) may depend on aqueous chemistry conditions.

4.6. Effects of nuclear decay

The incorporation of hundreds of thousands of radiocesium atoms (Sassi et al., 2017a) in radioactive soil particles raises questions about the possible effects of radioactive decay on the mineral structure, stability and the long–term fate and transport of Cs, both stable and radioactive. In this section, we focus only on two major processes occurring during ^{137}Cs beta–decay, namely transmutation and the emission of a high–energy beta–particle. In addition to the obvious safety issues, the lack of experimental investigations is in part due to time–- limitation by the half–life of the radioisotope. A useful feature of computational simulations in this case is that they enable the arbitrary acceleration of radioactive decay reactions.

Transmutation involves a chemical and oxidation state change of a compound such as an adsorbed Cs ion. The consequences of these changes have been investigated by ab initio calculations for interlayer radiocesium sorbed in phlogopite (Sassi et al., 2017b). Fig. 9 shows that the sudden appearance of Ba^{2+} highly destabilizes phlogopite by 4.3 eV with respect to interlayer radiocesium. The destabilizing energy is primarily due to the presence of a (+2) cation in a (+1) interlayer site. In addition, thermodynamic analysis indicates that Cs vacancies are more favorable than K and H vacancies by 0.1 and 2 eV respectively. These results have two consequences: (i) radiocesium transmutation appears to provide a means to weaken the binding of other Cs by favoring and accelerating its desorption, and (ii) a cation vacancy (K or Cs) is needed to accommodate the charge difference. If radiocesium concentrations in a clay particle are small, K desorption would occur more frequently than Cs desorption. However, the aforementioned recent experimental (Kogure et al., 2012; Okumura et al., 2014b; Tamura et al., 2014) and theoretical studies (Okumura et al., 2014a; Ruiz Pestana et al., 2017), which indicate that Cs ions tend to form Cs dense interlayers in a clay particle, suggest the possibility that Cs^{+} transmutation to Ba^{2+} could lead to progressive re–release of residual parent isotope.

The incidence of a high energy beta–particle on defect formation processes in clay minerals has been investigated by determining the threshold displacement energy (TDE) for various atoms in vermiculite from FPMD simulations (Sassi et al., 2016). The results indicate that Mg sites are the most radiation resistant while H sites are the most vulnerable. If the energy transferred by a beta–particle colliding with an atom in vermiculite is higher than the TDE of that site, then Fig. 9 shows the most frequently encountered Frenkel defect structure obtained at the end of the simulation. While

displaced Mg atoms generally end at the center of a siloxane ring, displaced tetrahedral Al or Si atoms promote ring opening and the formation of larger rings made of two adjacent rings. For displaced O atoms, siloxane rings can either open or remain closed by creating Si–Si or Al–Si bonds.

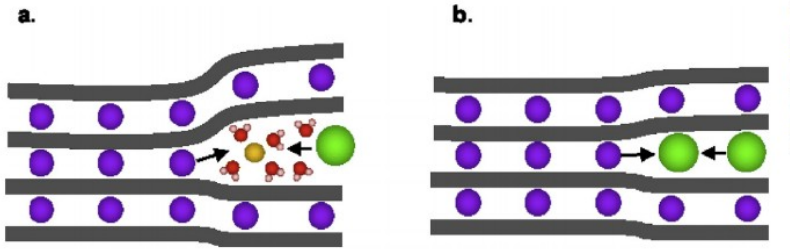

Fig. 8. Schematic of interlayer ion exchange pathway for Cs^+, including (a) decollapse–driven exchange of a solvated counterion (orange) and Cs^+ (light green) for K^+ (purple), and (b) direct exchange (right). (For interpretation of the references to color in this figure legend, the reader is referred to the Web version of this article.)

These results provide information about structural alterations associated with nuclear decay and their potential impact on the stability of interlayer Cs. Because the density of defects created by nuclear decay reactions obviously will depend on the concentration and distribution of radiocesium in soil, the results should motivate further experimental and theoretical investigations. For example, experiments involving ^{134}Cs at different concentrations could be used as a proxy to accelerate the consequences of ^{137}Cs decay and examine the thermodynamics and kinetics of ion–exchange processes in contaminated soil minerals.

5. Discussion regarding waste–soil volume reduction

Here, we discuss strategies to reduce the volume of waste soils based on microscopic insights reviewed above. One of the most important insights is that radiocesium adsorbs strongly in the anhydrous interlayers of illite or weathered biotite and that the adsorbed form is quite robust against chemical and physical attack. This suggests that effective waste volume reduction likely requires physical fractionation of the waste soils into phyllosilicate minerals (particularly biotite and illite) and other solid fractions. Such a physical separation, if possible, should yield a dramatic reduction of the contaminated soil volume. One possible separation scheme involving superconducting coils acting on the intrinsic magnetic moment of biotite may be promising. However, iron is distributed in a complex manner within the octahedral sheets, because biotite is a part of solution solid series. The details could be clarified by atomic level calculations aided by experiments. The question regarding whether or not there is a useful correlation to be exploited between the magnetic moment and radioactivity remains open and worthy of exploration.

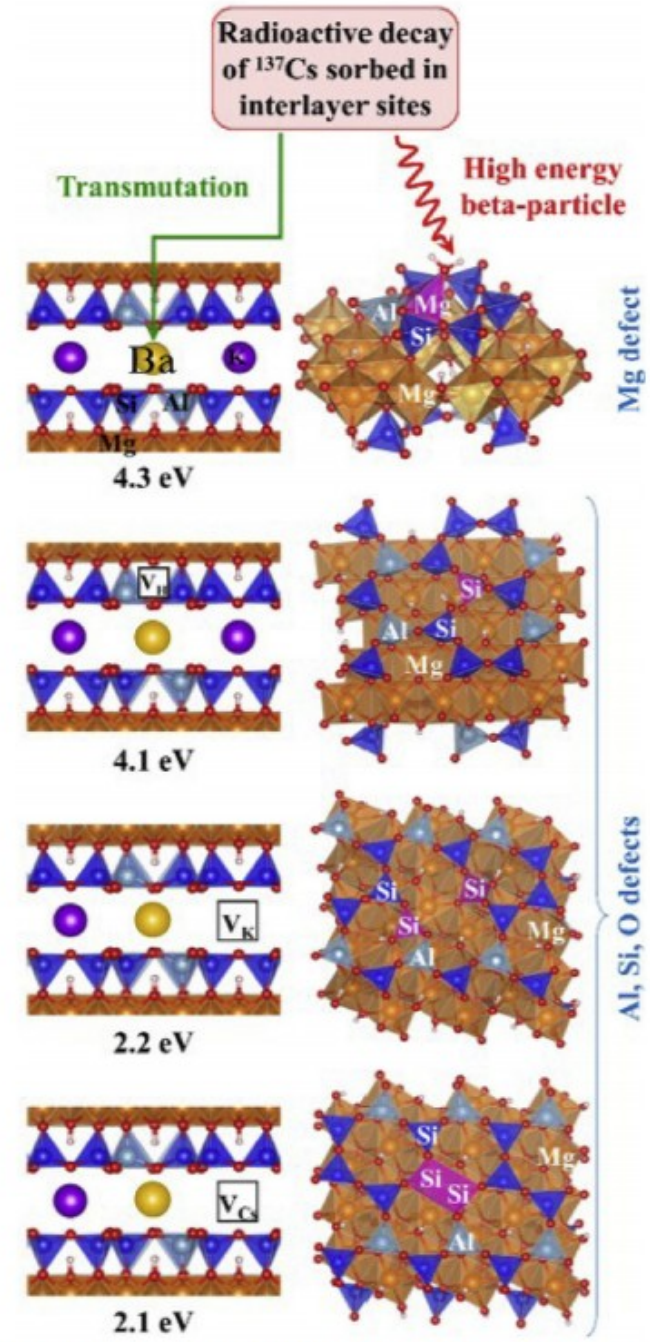

Fig. 9. Overview of radiocesium decay induced defects in phlogopite (left) and vermiculite (right). (left) Calculated thermodynamics for the creation of charge compensating defects with respect to the energy of an interlayer sorbed radiocesium (i.e. before transmutation). (right) Example of the most frequently encountered defect structures obtained at the end of simulation for displacement energy above the TDE values of the given specie. The magenta polyhedron highlights the structure of the defect. Adapted from (Sassi et al., 2016, Fig. 3). Reproduced with kind permission of The Clay Minerals Society, publisher of Clays and Clay Minerals. SiO_4 tetrahedra are shown in dark blue, AlO_4 and AlO_6 polyhedra in light blue, MgO_6 octahedra in brown, and O, H, K, and Ba atoms are shown by red, light pink, purple, and yellow spheres, respectively. (For interpretation of the references to color in this figure legend, the reader is referred to the Web version of this article.)

Further volume reduction, if necessary, will likely require radiocesium extraction from the phyllosilicate particles. Extraction schemes proposed for biotite consist of either chemical or physical treatments. In the former, two directions exist, i.e., the extraction without and with destruction of the mineral framework. The most obvious non–- destructive chemical method, extraction by cation exchange, is supported by a long history. Unfortunately, the strong adsorption selectivity and very slow reversibility of adsorption on FES and in anhydrous interlayers implies that a significant fraction of radiocesium may be highly recalcitrant to this method on reasonable time–scales.

Destructive chemical treatments involve the dissolution of the biotite framework. Surprisingly, strong acids are not enough for complete desorption from weathered biotite, at least under ambient conditions with reasonable short periods. An alternative chemical method involving incineration with alkali salts has been shown to yield up to 100% radiocesium extraction, but at a prohibitively high cost (Shimoyama et al., 2014; Honda et al., 2017), illustrating the need for additional research and optimization.

As for physical extraction methods, one proposed scheme involves use of milling to destroy the phyllosilicate framework. This technique has shown promising results in well–controlled conditions, but it requires specific conditions (such as grain size homogeneity) to perform effectively in reasonable periods. More insights would be beneficial to optimize this approach.

Finally, beyond radiocesium extraction and volume reduction, reuse of the residual decontaminated waste soil is an important relevant consideration, because huge amounts of residual contaminated material below acceptable radioactivity levels is likely to remain in all cases. If this residual waste soil contains sufficiently low radiocesium levels, its safe isolation from the environment may be achievable through its use as fill for embankments coated by concrete, or as aggregate for concrete. In these cases, the long–term fate of trace levels of entrapped radiocesium should be studied, for example through a combination of experiments and atomic–scale calculation techniques such as those reviewed above.

6. Conclusions

We have reviewed key experimental knowledge and recent developments enabled by computational molecular modeling on clay particles interacting with radiocesium, emphasizing the advances driven by the environmental fate, transport and remediation challenges associated with the FDNPP accident. Overall, state–of–the–art numerical simulations provide detailed insight into the role of microstructural details in controlling Cs adsorption on phyllosilicate minerals, particularly in regards to the atomic–scale and long time–scale processes that are difficult to access by experiment. The scientific understanding in this area continues to progress rapidly owing to the

concerted application of advanced experimental and high–performance computational research.

The research reviewed above illustrates three key strengths of computational molecular modeling. The first is the ability to directly access the mechanism of Cs adsorption by easily testing various hypotheses. The second is the ability to evaluate key quantities such as free energies of adsorption on individual surface sites, time constants of radiocesium diffusion, and desorption probabilities of Cs leaching caused by radiation damage. The third is that atomistic simulations provide a safe and economical platform for the study of radioactive or other hazardous substances.

Despite the favorable features summarized above, one should keep in mind that, not unlike experiments, atomistic–level simulations remain inherently sensitive to the approximations made in their implementation. In particular, they require a priori knowledge of the structure of various possible adsorption sites. In the case of classical MD simulations, they also require the use of semi–empirical interatomic potential parameters. As in other scientific areas, advances in computational modeling of radiocesium adsorption go hand–in–hand with microscopic–scale experimental studies: the iteration between modeling and experiments yields lasting insights.

As a final comment, it is worth noting that decisions on waste soil management should, in principle, be based on reliable scientific insights. In this review, we believe we have shown that molecular simulation can contribute effectively to obtaining such insights.

Acknowledgments

This work was partially supported by JAEA-PNNL and JAEA-UCBLBNL collaborative projects, JAEA-NIMS cooperative project organized by T. Yaita, and F-Trace project. This work was also partially supported by JSPS-KAKENHI Grant Number 16H02437 to M.O. and M.M., by the US DOE Office of Science, Office of Basic Energy Sciences (CSGB Division) under Award Number DE-SC0018419 to I.B. M.O. and M.M. would thank the director of CCSE, Dr. H. Takemiya, and all other staff members. M.O. would also thank Prof. T. Kogure, Dr. I. Shimoyama, Prof. Y. Takahashi, and Dr. T. Yaita for fruitful discussion on clay minerals and their properties of cesium adsorption.

References

Araki, Y., Satoh, H., Okumura, M., Onishi, H., 2017. Localization of cesium on montmorillonite surface investigated by frequency modulation atomic force microscopy. Surf. Sci. 665, 32–36.

Barshad, I., 1954. Cation exchange in micaceous minerals: II. Replaceability of ammonium and potassium from vermiculite, biotite, and montmorillonite. Soil Sci. 78, 57–76.

Benedicto, A., Missana, T., Fernández, A.M., 2014. Interlayer collapse affects on cesium adsorption onto illite. Environ. Sci. Technol. 48, 4909–4915.

Bickmore, B., et al., 2003. Ab initio determination of edge surface structures for dioctahedral 2:1 phyllosilicates: implications for acid–base reactivity. Clay Clay Miner. 51, 359–371.

Bostick, B.C., Vairavamurthy, M.A., Karthikeyan, K.G., Chorover, J., 2002. Cesium adsorption on clay minerals: an EXAFS spectroscopic investigation. Environ. Sci. Technol. 36, 2670–2676.

Bourg, I.C., Lee, S., Fenter, P., Tournassat, C., 2017. Stern layer structure and energetics at mica–water interfaces. J. Phys. Chem. C 121, 9402–9412.

Bourg, I.C., Sposito, G., 2010. Connecting the molecular scale to the continuum scale for diffusion processes in smectite–rich porous media. Environ. Sci. Technol. 44, 2085–2091.

Bourg, I.C., Sposito, G., 2011. Molecular dynamics simulations of the electrical double layer on smectite surfaces contacting concentrated mixed electrolyte (NaCl–CaCl2) solutions. J. Colloid Interface Sci. 360, 701–715.

Bourg, I.C., Sposito, G., Bourg, A.C.M., 2007. Modeling the acid–base surface chemistry of montmorillonite. J. Colloid Interface Sci. 312, 297–310.

Bradbury, M., Baeyens, B., 2000. A generalised sorption model for the concentration dependent uptake of caesium by argillaceous rocks. J. Contam. Hydrol. 42, 141–163.

Brouwer, E., Baeyens, B., Maes, A., Cremers, A., 1983. Cesium and rubidium ion equilibriums in illite clay. J. Phys. Chem. 294, 1213–1219.

Carroll, S., Walther, J., 1990. Kaolinite dissolution at 25°, 60°, and 8°C. Am. J. Sci. 290, 797–810.

Churakov, S., 2006. Ab initio study of sorption on pyrophyllite: structure and acidity of the edge sites. J. Phys. Chem. B 110, 4135–4146.

Comans, R., Haller, M., De Preter, P., 1991. Sorption of cesium on illite: non–equilibrium behaviour and reversibility. Geochem. Cosmochim. Acta 55, 433–440.

Comans, R., Hockley, D., 1992. Kinetics of cesium sorption on illite. Geochem. Cosmochim. Acta 56, 3217–3227.

Cornell, R., 1993. Adsorption of Cs on minerals –A review. J. Radioanal. Nucl 171, 483–500.

Cremers, A., Pleysier, J., 1973. Adsorption of the silver–thiourea complex in montmorillonite. Nature 243, 86–87.

Cygan, R., Liang, J., Kalinichev, A., 2004. Molecular models of hydroxide, oxyhydroxide, and clay phases and the development of a general force field. J. Phys. Chem. B 108, 1255–1266.

de Koning, A., Comans, R., 2004. Reversibility of radiocaesium sorption on illite. Geochem. Cosmochim. Acta 68, 2815–2823.

Delvaux, B., Kruyts, N., Maes, E., Smolders, E., 2000. Fate of radiocesium in soil and rhizosphere. In: Gobran, G.R., Wenzel, W.W., Lombi, E. (Eds.), Trace Elements in the Rhizosphere. CRC Press, London, pp. 61–91.

Evans, D., Alberts, J., Clark III, R., 1983. Reversible ion–exchange fixation of cesium–137 leading to mobilization from reservoir sediments. Geochem. Cosmochim. Acta 47, 1041–1049.

Fan, Q., Tanaka, M., Tanaka, K., Sakaguchi, A., Takahashi, Y., 2014a. An EXAFS study on the effects of natural organic matter and the expandability of clay minerals on cesium adsorption and mobility. Geochem. Cosmochim. Acta 135, 49–65.

Fan, Q., Yamaguchi, N., Tanaka, M., Tsukada, H., Takahashi, Y., 2014b. Relationship between the adsorption species of cesium and radiocesium interception potential in soils and minerals: an EXAFS study. J. Environ. Radioact. 138, 92–100.

Fuller, A.J., Shaw, S., Ward, M.B., Haigh, S.J., Mosselmans, J.F.W., Peacock, C.L., Stackhouse, S., Dent, A.J., Trivedi, D., Burke, I.T., 2015. Caesium incorporation and retention in illite interlayer. Appl. Clay Sci. 108, 128–134.

Goto, M., Rosson, R., Wampler, J.M., Elliott, W.C., Serkiz, S., Kahn, B., 2008. Freundlich and dual Langmuir isotherm models for predicting 137Cs binding on Savannah River Site soils. Health Phys. 94, 18–32.

Heinz, H., Koerner, H., Anderson, K.L., Vaia, R.A., Farmer, B.L., 2005. Force field for mica–type silicates and dynamics of octadecylammonium chains grafted to montmorillonite. Chem. Mater. 17, 5658–5669.

Honda, M., Shimoyama, I., Okamoto, Y., Baba, Y., Suzuki, S., Yaita, T., 2016. X–ray absorption fine structure at the cesium L3 absorption edge for cesium sorbed in clay minerals. J. Phys. Chem. C 120, 5534–5538.

Honda, M., Okamoto, Y., Shimoyama, I., Shiwaku, H., Suzuki, S., Yaita, T., 2017. Mechanism of Cs removal from Fukushima weathered biotite by heat treatment with a NaCl–CaCl2 mixed salt. ACS Omega 2, 721–727.

Iannuzzi, M., Laio, A., Parrinello, M., 2003. Efficient exploration of reactive potential energy surfaces using Car–Parrinello molecular dynamics. Phys. Rev. Lett. 90, 238302.

Ikeda, T., 2016. First–principles–based simulation of interlayer water and alkali metal ions in weathered biotite. J. Chem. Phys. 145, 124703.

Ikeda, T., Boero, M., 2012. Hydration structure and polarization of heavy alkali ions: a first principles molecular dynamics study of Rb+ and Cs+. J. Chem. Phys. 137 041101.

Ikeda, T., Suzuki, S., Yaita, T., 2015. Characterization of adsorbed alkali metal ions in 2:1 type clay minerals from first–principles metadynamics. J. Phys. Chem. 119, 8369–8375.

International Atomic Energy Agency, 2015. The Fukushima Daiichi Accident. Report by the Director General. . http://www-pub.iaea.org/MTCD/Publications/ PDF/ Pub1710-ReportByTheDG-Web.pdf (accessed 16 January 2018).

Jackson, M.L., 1963. Interlayering of expansible layer silicates in soils by chemical weathering. Clay Clay Miner. 11, 29–46.

Jacobs, D.G., Tamura, T., 1960. The mechanism of ion fixation using radio–isotope techniques. In: In: van Baren, F.A. (Ed.), Transactions 7th International Congress of Soil Science, vol. 2. The International Society of Soil Science, Amsterdam, pp. 206–214.

Japan Atomic Energy Agency, 2014a. Remediation of Contaminated Areas in the Aftermath of the Accident at the Fukushima Daiichi Nuclear Power Station: Overview, Analysis and Lessons Learned, 1; a Report on the “decontamination Pilot Project”. JAEA–Review 2014–051. . https://doi.org/10.11484/jaea-review-2014- 051.

Japan Atomic Energy Agency, 2014b. Remediation of Contaminated Areas in the Aftermath of the Accident at the Fukushima Daiichi Nuclear Power Station; Overview, Analysis and Lessons Learned, 2; Recent Developments, Supporting R&D and International Discussions. JAEA–Review 2014–052. https://doi.org/10.11484/ jaea-review-2014-052.

Japan Meteorological Agency, 2011. The 2011 Great East Japan Earthquake – Portal–. http://www.jma.go.jp/jma/en/2011_Earthquake/2011_Earthquake.html (accessed 16 January 2018).

Kerisit, S., Okumura, M., Rosso, K., Machida, M., 2016. Molecular simulation of cesium adsorption at the basal surface of phyllosilicate minerals. Clay Clay Miner. 64, 389–400.

Kikuchi, R., Mukai, H., Kuramata, C., Koura, T., 2015. Cs–sorption in weathered biotite from Fukushima granitic soil. J. Mineral. Petrol. Sci. 110, 126–134.

Kim, Y., Kirkpatrick, R.J., Cygan, R.T., 1996. 133Cs NMR study of cesium on the surfaces of kaolinite and illite. Geochem. Cosmochim. Acta 60, 4059–4074.

Kim, Y., Kirkpatrick, R.J., 1997. 23Na and 133Cs NMR study of cation adsorption on mineral surfaces: local environments, dynamics, and effects of mixed cations. Cosmochim. Acta 61, 5199–5208.

Kogure, T., Morimoto, K., Tamura, K., Sato, H., Yamagishi, A., 2012. XRD and HRTEM evidence for fixation of cesium ions in vermiculite clay. Chem. Lett. 41, 380–382.

Kosakowski, G., Churakov, S., Thoenen, T., 2008. Diffusion of Na and Cs in montmorillonite. Clay Clay Miner. 56, 190–206.

Kubicki, J. (Ed.), 2016. Molecular Modeling of Geochemical Reactions: an Introduction. Wiley, West Sussex.

Kuwahara, Y., 2006. In–situ AFM study of smectite dissolution under alkaline conditions at room temperature. Am. Mineral. 91, 1142–1149.

Kwon, K., Newton, A., 2016. Structure and stability of pyrophyllite edge surfaces: effect of temperature and water chemical potential. Geochem. Cosmochim. Acta 190, 100–114.

Laio, A., Parrinello, M., 2002. Escaping free–energy minima. Proc. Natl. Acad. Sci. U.S.A. 99, 12562–12566.

Lammers, L.N., Bourg, I.C., Okumura, M., Kolluri, K., Sposito, G., Machida, M., 2017. Molecular dynamics simulations of cesium adsorption on illite nanoparticles. J. Colloid Interface Sci. 490, 608–620.

Lee, S., Fenter, P., Nagy, K., Sturchio, N., 2012. Monovalent ion adsorption at the muscovite (001)–solution interface: relationships among ion coverage and speciation, interfacial water structure, and substrate relaxation. Langmuir 28, 8637–8650.

Lee, S., Fenter, P., Nagy, K., Sturchio, N., 2013. Changes in adsorption free energy and speciation during competitive adsorption between monovalent cations at the muscovite (001) –water interface. Geochem. Cosmochim. Acta 123, 416–426.

Lee, S., Fenter, P., Nagy, K., Sturchio, N., 2017. Real–time observation of cation exchange kinetics and dynamics at the muscovite–water interface. Nat. Commun. 8, 15826.

Liebau, F., 1985. Structural Chemistry of Silicates. Springer–Verlag, Berlin.

Liu, C., Zachara, J.M., Smith, S.C., McKinley, J.P., Ainsworth, C.C., 2003. Desorption kinetics of radiocesium from subsurface sediments at Hanford Site, USA. Geochem. Cosmochim. Acta 67, 2893–2912.

Liu, X., Lu, X., Wang, R., Zhou, H., 2008. Effects of layer–charge distribution on the thermodynamic and microscopic properties of Cs–smectite. Geochem. Cosmochim. Acta 72, 1837–1847.

Liu, X., Cheng, J., Sprik, M., Lu, X., Wang, R., 2014. Surface acidity of 2:1–type dioctahedral clay minerals from first principles molecular dynamics simulations. Geochem. Cosmochim. Acta 140, 410–417.

Liu, X., Lu, X., Cheng, J., Sprik, M., Wang, R., 2015. Temperature dependence of interfacial structures and acidity of clay edge structures. Geochem. Cosmochim. Acta 160, 91–99.

Loganathan, N., Kalinichev, A., 2017. Quantifying the mechanisms of site–specific ion exchange at an inhomogeneously charged surface: case of Cs+/K+ on hydrated muscovite mica. J. Phys. Chem. C 121, 7829–7836.

Machida, M., Okumura, M., Nakamura, H., Sakuramoto, K., 2015. First-principles Calculation Studies on Cesium in Environmental Situations: Hydration Structures and Adsorption on Clay Minerals. Proceedings of Joint International Conference on Mathematics and Computation, Supercomputing in Nuclear Applications and the Monte Carlo Method (M&C + SNA + MC 2015) (CD-ROM).

Marry, V., Turq, P., Cartailler, T., Levesque, D., 2002. Microscopic simulation of structure and dynamics of water and counterions in a monohydrated montmorillonite. J. Chem. Phys. 111, 3435–3463.

Marry, V., Turq, P., 2003. Microscopic simulations of interlayer structure and dynamics in bihydrated heteroionic montmorillonite. J. Phys. Chem. B 107, 1832–1839.

Marry, V., Rotenberg, B., Turq, P., 2008. Structure and dynamics of water at a clay surface from molecular dynamics simulation. Phys. Chem. Chem. Phys. 10, 4802–4813.

Matsumura, D., Kobayashi, T., Miyazaki, Y., Okajima, Y., Nishihata, Y., Yaita, T., 2014. Real–time–resolved X–ray absorption fine structure spectroscopy for cesium adsorption on some clay minerals. Clay Sci. 18, 99–105.

McKinley, J.P., Zeissler, C.J., Zachara, J.M., Serne, R.J., Lindstrom, R.M., Schaef, H.T., Orr, R.D., 2001. Distribution and retention of 137Cs in sediments at the hanford site. Washington. Environ. Sci. Technol 35, 3433–3441.

McKinley, J.P., Zachara, J.M., Heald, S.M., Dohnalkova, A., Newville, M.G., Sutton, S.R., 2004. Microscale distribution of cesium sorbed to biotite and muscovite. Environ. Sci. Technol. 38, 1017–1023.

Meunier, A., 2006. Why are clay minerals small? Clay Miner. 41, 551–566.

Mikami, S., Maeyama, T., Hoshide, Y., Sakamoto, R., Sato, S., Okuda, N., Demongeot, S., Gurriaran, R., Uwamino, Y., Kato, H., Fujiwara, M., Sato, T., Takemiya, H., Saito, K., 2015. Spatial distributions of radionuclides deposited onto ground soil around the Fukushima Dai–ichi Nuclear Power Plant and their temporal change until December 2012. J. Environ. Radioact. 139, 320–343.

Ministry of Education, Culture, Sports, Science and Technology, 2011. Extension Site of Distribution Map of Radiation Dose, Etc. http://ramap.jmc.or.jp/map/eng/ (accessed 16 January 2018).

Ministry of Environment, 2011. Environment Remediation. http://josen.env.go.jp/en/ (accessed 16 January 2018).

Miyahara, K., McKinley, I.G., Saito, K., Hardie, S.M.L., Iijima, K., 2015. Use of Knowledge and Experience Gained from the Fukushima Daiichi Nuclear Power Station Accident to Establish the Technical Basis for Strategic Off–site Response. JAEA–Review 2015–001. https://doi.org/10.11484/jaea-review-2015-001.

Motokawa, R., Endo, H., Yokoyama, S., Nishitsuji, S., Kobayashi, T., Suzuki, S., Yaita, T., 2014a. Collective structural changes in vermiculite clay suspensions induced by cesium ions. Sci. Rep. 4, 6585.

Motokawa, R., Endo, H., Yokoyama, S., Ogawa, H., Kobayashi, T., Suzuki, S., Yaita, T., 2014b. Mesoscopic structures of vermiculite and weathered biotite clays in suspension with and without cesium ions. Langmuir 30, 15127–15134.

Micas: crystal chemistry & metamorphic petrology. In: In: Mottana, A., Sassi, F.P., Thompson Jr.J.B., Guggenheim, S. (Eds.), Reviews in Mineralogy & Geochemistry, vol 46 The Mineralogical Society of America, Washington, DC.

Mukai, H., Hatta, T., Kitazawa, H., Yamada, H., Yaita, T., Kogure, T., 2014. Speciation of radioactive soil particles in the Fukushima contaminated area by IP autoradiography and microanalyses. Environ. Sci. Technol. 48, 13053–13059.

Mukai, H., Motai, S., Yaita, T., Kogure, T., 2016a. Identification of the actual cesium–adsorbing materials in the contaminated Fukushima soil. Appl. Clay Sci. 121–122, 188–193.

Mukai, H., Hirose, A., Motai, S., Kikuchi, R., Tanoi, K., Nakanishi, M.T., Yaita, T., Kogure, T., 2016b. Cesium adsorption/desorption behavior of clay minerals considering actual contamination conditions in Fukushima. Sci. Rep. 6 21543.

Ngouana, B.F., Kalinichev, A.G., 2014. Structural arrangements of isomorphic substitution in smectites: molecular simulation of the swelling properties, interlayer structure, and dynamics of hydrated Cs–Montmorillonite revisited with new clay models. J. Phys. Chem. C 118, 12758–12773.

Okumura, M., Kerisit, S., Rosso, K., Machida, M., 2017. Origin of 6–fold coordinated aluminum at (010)–type pyrophyllite edges. AIP Adv. 7 055211.

Okumura, M., Nakamura, H., Machida, M., 2013. Mechanism of strong affinity of clay minerals to radioactive cesium: first–principles calculation study for adsorption of cesium at frayed edge sites in muscovite. J. Phys. Soc. Jpn. 82 033802.

Okumura, M., Nakamura, H., Machida, M., 2014a. Energetics of atomic level serial ion exchange for cesium in micaceous clay minerals. Clay Sci. 18, 53–61.

Okumura, T., Tamura, K., Fujii, E., Yamada, H., Kogure, T., 2014b. Direct observation of cesium at the interlayer region in phlogopite mica. Microscopy 63, 65–72.

Pintea, S., de Poel, W., de Jong, A.E.F., Vonk, V., van der Asdonk, P., Drnec, J., Balmes, O., Isern, H., Dufrane, T., Felici, R., Vlieg, E., 2016. Solid–liquid interface structure of muscovite mica in CsCl and RbBr solutions. Langmuir 32, 12955–12965.

Pitman, M.C., van Duin, A.C.T., 2012. Dynamics of confined reactive water in smectite clay–zeolite composites. J. Am. Chem. Soc. 134, 3042–3053.

Poinssot, C., Baeyens, B., Bradbury, M., 1999. Experimental and modelling studies of caesium sorption on illite. Geochem. Cosmochim. Acta 63, 3217–3227.

Qin, H., Yokoyama, Y., Fan, Q., Iwatani, H., Tanaka, K., Sakaguchi, A., Kanai, Y., Zhu, J., Onda, Y., Takahashi, Y., 2012. Investigation of cesium adsorption on soil and sediment samples from Fukushima Prefecture by sequential extraction and EXAFS technique. Geochem. J. 46, 297–302.

Quirk, J., Chute, J., 1968. Potassium release from mica–like clay minerals. In: 9th International Congress of Soil Science Transactions. International Society of Soil Science, Adelaide, pp. 671–681.

Rajec, P., Sucha, V., Eberl, D.D., Srodon, J., Elsass, F., 1999. Effect of illite particle shape on cesium sorption. Clay Clay Miner. 47, 755–760.

Rausell–Colom, J., Sweatman, T., Wells, C., Norrish, K., 1965. Studies in the artificial weathering of mica. In: Experimental Pedology. Butterworth, London, pp. 40–72.

Reichenbach, H., Rich, C., 1968. Preparation of dioctahedral vermiculites from muscovite and subsequent exchange properties. In: 9th International Congress of Soil Science Transactions. Elsevier, New York, pp. 709–719.

Reichenbach, H., Rich, C., 1969. Potassium release from muscovite as influenced by particle size. Clay Clay Miner. 17, 23–29.

Rosso, K., Rustad, J., Bylaska, E., 2001. The Cs/K Exchange in muscovite interlayers: an ab initio treatment. Clay Clay Miner. 49, 500–513.

Rotenberg, B., Marry, V., Dufreche, J.F., Malikova, N., Giffaut, E., Turq, P., 2007. Modeling water and ion diffusion in clays: a multiscale approach. C. R. Chim 10, 1108–1116.

Rotenberg, B., Morel, J.–P., Marry, V., Turq, P., Morel–Desrosiers, N., 2009. On the driving force of cation exchange in clays: insights from combined microcalorimetry experiments and molecular simulation. Geochem. Cosmochim. Acta 73, 4034–4044.

Ruiz Pestana, L., Kolluri, K., Head–Gordon, T., Lammers, L., 2017. Direct exchange mechanism for interlayer ions in non–swelling clays. Environ. Sci. Technol. 51, 393–400.

Sánchez–Pastor, N., Aldushin, K., Jordan, G., Schmahl, W., 2010. K+–Na+ exchange in phlogopite on the scale of a single layer. Geochem. Cosmochim. Acta 74, 1954–1962.

Sakuma, H., Kawamura, K., 2011. Structure and dynamics of water on Li+–, Na+–, K+–, Cs+–, H3O+–exchanged muscovite surfaces: a molecular dynamics study. Geochem. Cosmochim. Acta 75, 63–81.

Sassi, M., Rosso, K., Okumura, M., Machida, M., 2017a. Reply to Comments on radiation–damage resistance in phylloscilicate minerals from first principles and implications for radiocesium and strontium retention in soils. Clay Clay Miner. 65, 371–375.

Sassi, M., Okumura, M., Machida, M., Rosso, K., 2017b. Transmutation effects on long–term Cs retention in phyllosilicate minerals from first principles. Phys. Chem. Chem. Phys. 19, 27007–27014.

Sassi, M., Rosso, K., Okumura, M., Machida, M., 2016. Radiation–damage resistance in phylloscilicate minerals from first principles and implications for radiocesium and strontium retention in soils. Clay Clay Miner. 64, 108–114.

Sawhney, B.L., 1966. Cesium sorption in relation to lattice spacing and cation exchange capacity of biotite. Soil Sci. Soc. Am. Proc. 31, 181–183.

Sawhney, B.L., 1972. Selective sorption and fixation of cations by clay minerals: a review. Clay Clay Miner. 20, 93–100.

Scott, A., Hunziker, R., Hanway, J., 1960. Chemical extraction of potassium from soils and micaceous minerals with solutions containing sodium tetraphenylboron. I. Preliminary experiments. Soil Sci. Soc. Am. J. 24, 191–194.

Scott, A., Smith, S., 1966. Susceptibility of interlayer potassium in micas to exchange with sodium. In: Clays and Clay Minerals, Proceedings of the Fourteenthe National Conference. Pergamon Press, Oxford, pp. 69–80.

Shimoyama, I., Hirao, N., Baba, Y., Izumi, T., Okamoto, Y., Yaita, T., Suzuki, S., 2014. Low–pressure sublimation method for cesium decontamination of clay minerals. Clay Sci. 18, 71–77.

Shroll, R.M., Smith, D.E., 1999. Molecular dynamics simulations in the grand canonical ensemble: application to clay mineral swelling. J. Chem. Phys. 111, 9025–9033.

Skipper, N.T., Refson, K., McConnell, J.D.C., 1989. Computer calculation of water–clay interactions using atomic pair potentials. Clay Miner. 24, 411–425.

Smith, D., 1998. Molecular computer simulations of the swelling properties and interlayer structure of cesium montmorillonite. Langmuir 14, 5959–5967.

Staunton, S., Roubaud, M., 1997. Adsorption of 137Cs on montmorillonite and illite; effect of charge compensating cation, ionic strength, concentration of Cs, K and fulvic acid. Clay Clay Miner. 45, 251–260.

Steefel, C.I., Carroll, S., Zhao, P., Roberts, S., 2003. Cesium migration in Hanford sediment: a multisite cation exchange model based on laboratory transport experiments. J. Contam. Hydrol. 67, 219–246.

Sutton, R., Sposito, G., 2001. Molecular simulation of interlayer structure and dynamics in 12.4 Å Cs–smectite hydrates. J. Colloid Interface Sci. 237, 174–184.

Sutton, R., Sposito, G., 2002. Animated molecular dynamics simulations of hydrated caesium–smectite interlayers. Geochem. Trans. 3, 73–80.

Tamura, K., Kogure, T., Watanabe, Y., Nagai, C., Yamada, H., 2014. Uptake of cesium and strontium ions by artificially altered phlogopite. Environ. Sci. Technol. 48, 5808–5815.

Takahashi, Y., Fan, Q., Suga, H., Tanaka, K., Sakaguchi, A., Takeichi, Y., Ono, K., Mase, K., Kato, K., Kanivets, V.V., 2017. Comparison of solid–water partitions of radiocesium in river waters in Fukushima and Chernobyl Areas. 12407. Sci. Rep. 7.

Tanaka, K., Watanabe, N., Yamasaki, S., Sakaguchi, A., Fan, Q., Takahashi, Y., 2018. Mineralogical control of the size distribution of stable Cs and radiocesium in riverbed sediments. Accepted for publication in. Geochem. J.

Tesson, S., Salanne, M., Rotenberg, B., Tazi, S., Marry, V., 2016. Classical polarizable force field for clays: pyrophyllite and talc. J. Phys. Chem. C 120, 3749–3758.

Tournassat, C., Davis, J.A., Chiaberge, C., Grangeon, S., Bourg, I.C., 2016. Modeling the acid–base properties of montmorillonite edge surfaces. Environ. Sci. Technol. 50, 13436–13445.

Tsuji, T., Matsumura, D., Kobayashi, T., Suzuki, S., Yoshii, K., Nishihata, Y., Yaita, T., 2014. Local structure around cesium in montmorillonite, vermiculite and zeolite under wet condition. Clay Sci. 18, 93–97.

Vasconcelos, I., Bunker, B., Cygan, R., 2007. Molecular dynamics modeling of ion adsorption to the basal surfaces of kaolinite. J. Phys. Chem. C 111, 6753–6762.

Wauters, J., Sweeck, L., Valcke, E., Elsen, A., Cremers, A., 1994. Availability of radiocaesium in solids: a new methology. Sci. Total Environ. 157, 239–248.

Wauters, J., Vidal, M., Elsen, A., Cremers, A., 1996. Prediction of solid/liquid distribution coefficients of radiocaesium in soils and sediments. Part two: a

new procedure for solid phase speciation of radiocaesium. Appl. Geochem. 11, 589–594.

White, G., Zelazny, L., 1988. Analysis and implications of the edge structure of dioctahedral phyllosilicates. Clay Clay Miner. 36, 141–146.

Whitley, H.D., Smith, D.E., 2004. Free energy, energy, and entropy of swelling in Cs-, Na-, and Sr–montmorillonite clays. J. Chem. Phys. 120, 5387–5395.

Yamada, H., Yokoyama, S., Watanabe, Y., Suzuki, M., Suzuki, S., Hatta, T., 2014. Cesium–adsorption behavior of weathered biotite from Fukushima Prefecture depends on the degree of vermiculitization. J. Ion Exch 25, 207–211.

Yoshida, N., Takahashi, Y., 2012. Land–surface contamination by radionuclides from the Fukushima Daiichi nuclear power plant accident. Elements 8, 201–206.

Young, D., Smith, D., 2000. Simulations of clay mineral swelling and hydration: Dependence upon interlayer ion size and charge. J. Phys. Chem. C 104, 9163–9170.

Zachara, J.M., Smith, S.C., Liu, C., McKinley, J.P., Serne, R.J., Gassman, P.L., 2002. Sorption of Cs+ to micaceous subsurface sediments from the Hanford site, USA. Geochem. Cosmochim. Acta 66, 193–211.

Zaunbrecher, L., Cygan, R., Elliott, W., 2015. Molecular models of cesium and rubidium adsorption on weathered micaceous minerals. J. Phys. Chem. 119, 5691–5700.

Zheng, Y., Zaoui, A., 2011. How water and counterions diffuse into the hydrated montmorillonite. Solid State Ionics 203, 80–85.

Zheng, Y., Zaoui, A., Shahrour, I., 2011. A theoretical study of swelling and shrinking of hydrated Wyoming montmorillonite. Appl. Clay Sci. 51, 177–181.